



Cobalt-Based Perovskites as Efficient Oxygen Exchange Redox Materials for Solar Thermochemical Application

Liuqing Yang¹, Hui Liu¹, Jianan Hao¹, Junshe Zhang¹ , and Jinjia Wei¹ 

¹ Xi'an Jiaotong University, China

*Correspondence: jjwei@mail.xjtu.edu.cn

Abstract. Solar thermochemical CO₂ splitting (STCS) cycles provide the promising routes to generate renewable fuel, fuel precursors, or chemical feedstocks by the utilization of renewable resources like solar thermal energy and CO₂ relating to current energy as well as climate change. Perovskites have been proposed as the potential oxygen exchange redox materials for the two-step STCS process due to their greater oxygen release and redox stability. Herein, the oxygen release and redox stability were investigated for the cobalt-based perovskites (SrCoO_{3-δ} and SrCo_{0.9}Zr_{0.1}O_{3-δ}) as the potential STCS candidates. Consequently, the XRD, FT-IR, and Raman confirmed the dual-phase perovskite constitutions of SrCo_{0.9}Zr_{0.1}O_{3-δ} (*i.e.* SrCoO_{2.29} and SrZrO₃) compared to SrCoO_{3-δ}. The thermogravimetric analysis indicated the incorporation of Zr could facilitate the oxygen release and enhance the phase stability. The near-equilibrium lattice oxygen release and uptake at high temperatures could be observed through the redox performance of SrCo_{0.9}Zr_{0.1}O_{3-δ} at different heating and cooling rates. The results are noteworthy and demonstrate the potential of Zr-enhanced cobalt-based perovskites as the oxygen exchange redox materials for practical solar thermochemical applications.

Keywords: Cobalt-Based Perovskites, Oxygen Exchange, Solar Energy

1. Introduction

The anthropogenic excessive CO₂ emissions resulting from the conventional utilization of fossil fuels have caused adverse effects on the global climate, environment and energy (*e.g.*, climate change, loss of biodiversity and energy insecurity). In this context, converting excess and nontoxic CO₂ into high-value-added chemicals and green carbonaceous fuels at a large enough scale is an essential strategy for the ambitious global carbon neutrality goal and the sustainable development of the environment and energy [1-3]. Among many emerging CO₂ conversion technologies, chemical looping processes have attracted considerable amounts of attention due to the inherent CO₂ capture, direct utilization and effective conversion process [4, 5]. Two-step solar thermochemical splitting of CO₂ (STCS) into platform chemicals (CO and O₂) involving the chemical looping principle provides an attractive route for the solar fuel production and CO₂ recycling due to the key features including the intrinsic operation at high temperatures, utilization of entire solar spectrum, and simplifying gas separation [6-8].

In the two-step thermochemical process, oxygen exchange redox materials (or oxygen carriers, OCs) are used to complete the reduction at high temperatures (T_{red}) and the re-oxidation by CO₂ at relatively lower temperatures (T_{ox}). Due to the flexibility of electronic and

crystal structure, the chemical versatility, the excellent redox reversibility, and the tunable thermodynamic characteristics, perovskite oxides have gained enormous recognition as promising OC candidates for the STCS process [9-12]. As the potential perovskites systems, cobalt-Based perovskites (e.g., $\text{SrCoO}_{3-\delta}$, LaCoO_3) was proposed as the OC candidate for the solar thermochemical application [13-15]. However, it is still imperative to further enhance the thermal stability, melting point, reaction kinetics and redox properties by various strategies in terms of the solar thermochemical application. Based on the reported works, Zr doping is beneficial to improve CO yield and thermochemical redox stability of material [16].

Herein, the Zr-doping $\text{SrCoO}_{3-\delta}$ as typical OC has been designed for the STCS process. The phase composition and stability as well as oxygen exchange capacity of the obtained samples in N_2 and air have been primarily comprehensively surveyed via various characterizations in the work. The observations demonstrated the optimized OC $\text{SrCo}_{0.9}\text{Zr}_{0.1}\text{O}_{3-\delta}$ which showed excellent thermal stability, and lattice oxygen release and uptake capacity.

2. Materials & Characterization

All OCs with the perovskite structure (SrCoO_3 and $\text{SrCo}_{0.9}\text{Zr}_{0.1}\text{O}_3$, denoted as SCO and SCZ91) were prepared by a typical sol-gel method in which adequate stoichiometric amounts of $\text{Sr}(\text{NO}_3)_2$, $\text{Co}(\text{NO}_3)_2 \cdot 6\text{H}_2\text{O}$, and $\text{Zr}(\text{NO}_3)_4 \cdot 5\text{H}_2\text{O}$ were dissolved into distilled water with citric acid, followed by adding ethylene glycol until the formation of viscous gel. Finally, the pristine samples were obtained by calcination at 400 °C and 1000 °C in air.

Subsequently, the crystal structures and chemical compositions of samples were investigated by XRD, FT-IR, and Raman in details. The thermodynamic equilibrium and reaction rate measurements were performed by adopting TGA procedures. For the TGA measurement, the optimal mass of sample (30.00 mg) was placed in an alumina crucible. An empty alumina crucible was used as the reference. The sample was purged with N_2 ($p_{\text{O}_2} \approx 10^{-5}$ bar, 50 mL/min) at 30 °C under atmospheric pressure. Afterward, the sample was heated and cooled to perform all of the measurements.

3. Results and discussion

3.1 Physicochemical characterization of OCs

The XRD patterns of as-prepared OCs are presented in Figure 1a. The pattern of the SCO powders can be indexed to a pure hexagonal structure ($\text{SrCoO}_{2.52}$). The synthesized SCZ91 adopts the cubic and orthorhombic mixed perovskite-type structure according to all peaks identified as the constituents of $\text{SrCoO}_{2.29}$ and SrZrO_3 , and no other impurity phases are detected. According to the magnified view from 30° to 35° (2θ) in Figure 1d, it is noted that an obvious peak shift toward a lower diffraction angle is induced by the incorporation of Zr.

The chemical structures and vibrational bonds of OCs were characterized by Fourier transform infrared spectroscopy (FT-IR) and Raman spectroscopy. In Figure 1b and e, the absorption bands at 400-450 cm^{-1} are allocated to metal cations bending and stretching vibrations of BO_6 (CoO_6 or ZrO_6) octahedron. The typical peaks at 570 cm^{-1} assigned to the metal-oxygen bond (Co-O and Zr-O) antisymmetric stretching vibration in the BO_6 octahedra of perovskite structure and the fingerprint of perovskite at 660 cm^{-1} can be observed [17,18]. Other absorption bands appearing around 857 cm^{-1} , 993-1202 cm^{-1} , and 1464 cm^{-1} indicate the twisting and stretching vibration of the corresponding carbonates and C-H bond emerging in the OCs (Figure 1e). Some other characteristic groups originating from the gaseous CO_2 in the atmosphere as well as the water adsorbed on samples or KBr are also observed in the FT-IR spectra (Figure 1b) [19]. All the above carbonates and adsorbed species could be neglected for the OCs. As shown in Figures 1c and f, SCO and SCZ91 show three different Raman modes in the displayed zone. The peaks at 110, 130 and 170 cm^{-1} are attributed to B_{2g} mode

related to the rotation of CoO_6 about the z-axis and CoO_4 bending, and Sr out-of-phase vibrations in the yz-plane, etc [20]. The peaks at 469 and 510 cm^{-1} are ascribed to the CoO_6 and CoO_4 bending vibrations, etc. The peaks at 628 and 677 cm^{-1} are assigned to the apical $\text{O}_{(2)}$ out-of-phase stretching in the yz-plane, CoO_6 breathing, etc. The theoretical and experimental ($25\text{ }^\circ\text{C}$) Raman modes for OCs are given in Table 1. The FT-IR and Raman analysis further confirmed the perovskite structure of pristine OCs.

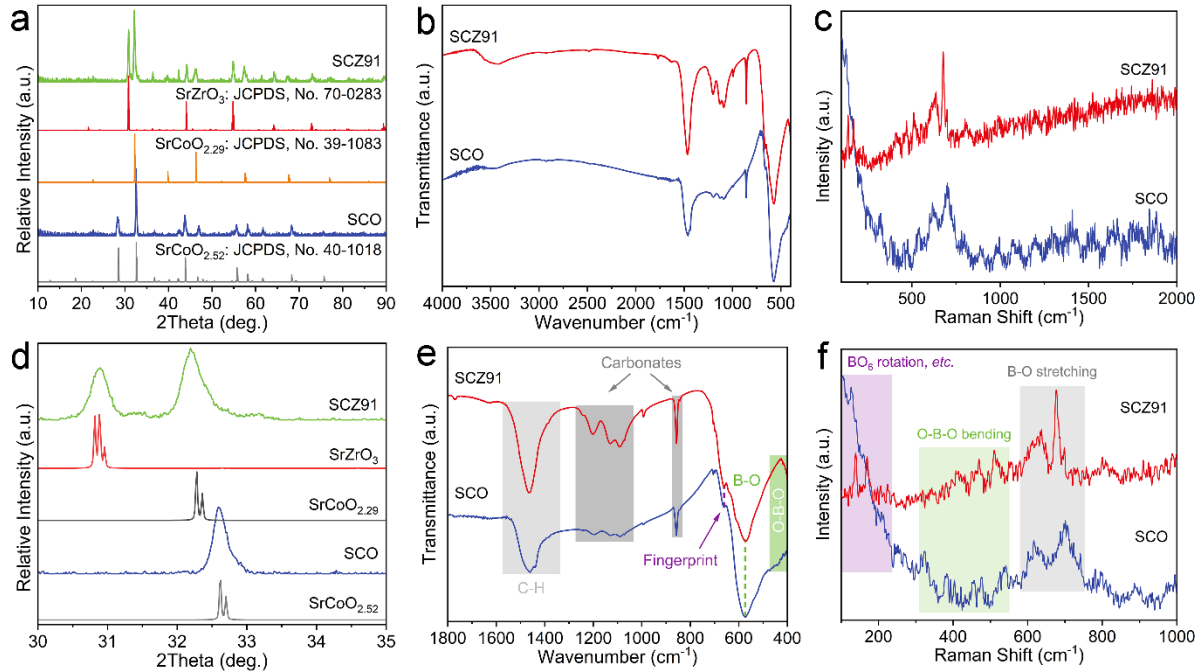


Figure 1. Characterizations of fresh OCs. (a, d) XRD patterns, (b, e) FT-IR spectra, (c, f) Raman spectra.

Table 1. Theoretical and experimental Raman modes for OCs.

Calc. (cm^{-1}) [20]	Expt. (cm^{-1})	Assignment
106	110	B_{2g} (CoO_6 rotation about the z-axis; CoO_4 bending; $\text{Co}_{(1)}$ and $\text{Co}_{(2)}$ out-of-phase vibrations along the x-axis; Sr out-of-phase vibrations along the x-axis)
122	130	B_{3g} (Sr out-of-phase vibrations in the yz-plane)
169	170	A_g (CoO_6 rotation about the x-axis; apical $\text{O}_{(2)}$ bending; $\text{Co}_{(1)}$ and $\text{Co}_{(2)}$ out-phase vibrations along the z-axis; Sr out-of-phase vibrations in the yz-plane)
471	469	A_g (CoO_6 and CoO_4 bending vibrations; $\text{Co}_{(1)}$ and $\text{Co}_{(2)}$ out-phase along the z-axis);
518	510	B_{3g} (CoO_6 bending; $\text{Co}_{(1)}$ and $\text{Co}_{(2)}$ out-phase vibrations along the z-axis)
629	628	A_g (apical $\text{O}_{(2)}$ out-of phase stretching in the yz-plane; $\text{Co}_{(1)}$ and $\text{Co}_{(2)}$ out-phase vibrations along the z-axis)
644	677	B_{3g} (CoO_6 breathing; apical $\text{O}_{(2)}$ out-of phase stretching in the yz-plane; $\text{Co}_{(1)}$ and $\text{Co}_{(2)}$ out-phase vibrations along the y-axis)

3.2 Phase transition and stability

Simultaneous thermogravimetry and differential scanning calorimetry (TG-DSC) measurements were performed under N₂ using a ramp rate of 10 °C/min to detect phase transitions and compare the mass change difference of OCs (Figure 2). For all OCs, mass loss behavior can be divided into three steps and performs the maximal variation in step III (Figure 2a), suggesting the efficient oxygen release of cobalt-based perovskites. The DSC data (Figure 1b) further reveal three phase transitions of SCO and the phase stability of SCZ91 at high temperatures [21]. Furthermore, it is to be noted that mass loss occurs predominantly before the phase transition (Figures 2a and b), implying the profound influence of Zr on the properties of SCO. In comparison, the mass loss of SCZ91 is higher than SCO in all steps (Figure 2c), indicating the incorporation of Zr contributed to the oxygen release. Due to the importance of oxygen release performance at higher temperatures (step III), the oxygen content is further calculated for two OCs (Figure 2d and Table 2), indicating the excellence of SCZ91. Compared to Zr⁴⁺-doped CeO₂, SCZ91 exhibits similar performances [22]. For the improvement of phase stability and oxygen content resulted from Zr doping, the possible mechanism is the decrease of oxygen vacancies and the crystallographic enhancement due to the introduction of quadrivalent doping ions Zr⁴⁺ [23]. Overall, based on the TG-DSC results, SCZ91 can be further evaluated as a potential oxygen carrier because this material not only stands to meet the oxygen release requirements for STCS applications due to the incorporation of Zr, but also benefits from a composition of cobalt-based perovskites.

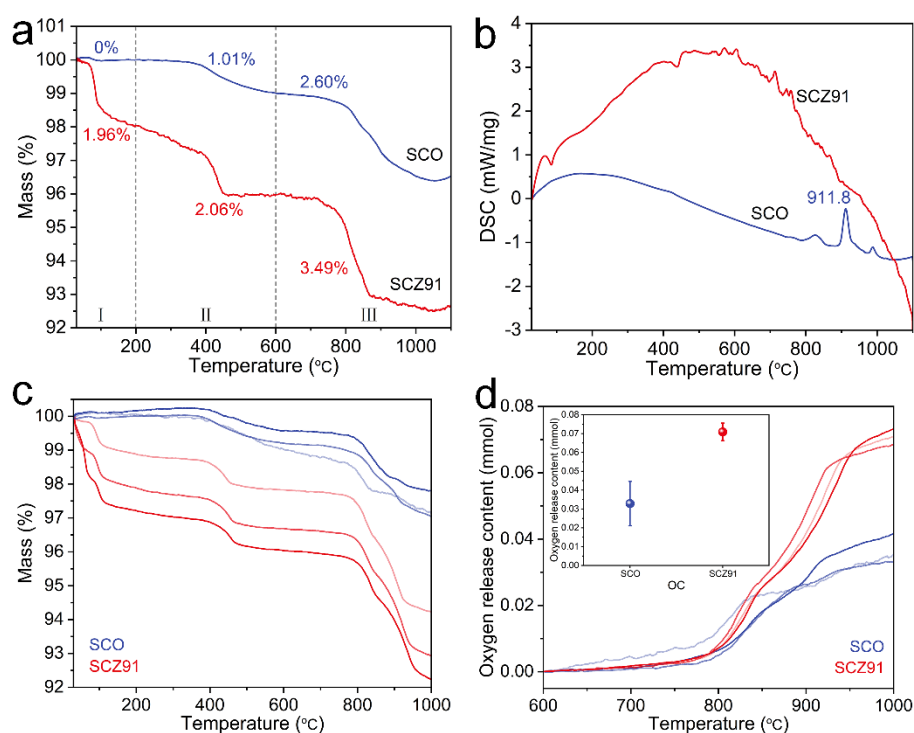


Figure 2. Thermal properties of fresh OCs. (a) mass profiles, (b) DSC profiles, (c) mass profiles of three measurements, (d) oxygen content change in step III (600 °C-1000 °C). Temperature ramp rate of 10 °C/min, about 30.00 mg in mass.

Table 2. Comparison of mass and oxygen content for OCs according to the TG-DSC measurements.

OC	Mass loss (%)	Mass loss in step III (%)	Oxygen content in step III (mmol)
SCO	2.6756 (±0.4199)	1.9467 (±0.2108)	0.038 (±0.012)
SCZ91	6.8717 (±1.0110)	3.7133 (±0.1250)	0.071 (±0.005)

3.3 Effects of heating and cooling rates on redox performance

For the STCS process, the heating and cooling rates as the important parameters, which involves the oxygen evolution rate, material sintering, external heat input capacity and equipment life span *etc.*, have been evaluated based on the reduction and oxidation rate analysis in the reduction and re-oxidation process, as shown in Figure 3. The reduction process of SCZ91 at different heating rates was divided into two stages, corresponding to a temperature-elevating stage from 30 to 1000 °C in N₂ and an isothermal stage at 1000 °C in N₂ (Figures 3a and c). The weight change is observed when the temperature increases from 30 °C to 200 °C, which can be attributed to the change of water adsorbed on the surface of OC. As the temperature increase from 400 °C to 600 °C, weight loss could be ascribed to the surface oxygen desorption from the sample. At temperatures above 750 °C, two high-temperature peaks are observed for OC, which is mainly concerned with the lattice oxygen. Based on the final isothermal stage, an average oxygen release content of 0.067 mmol is obtained for the lattice oxygen (600 °C-1000 °C, Figure 3b).

The re-oxidation reaction of SCZ91 at different cooling rates in air was conducted from 1000 to 500 °C (Figure 3d-f). It can be noted that the final re-oxidation degree with the cooling rates is about ~ 0.034 mmol compared with the temperature-elevating stage (Figure 3e), which may be attributed to the fast decrease of temperature to inadequate oxygen replenishment. Thus, the rate of 10 °C/min may be an optimal cooling rate based on the re-oxidation time and the final re-oxidation degree. By differentiating the oxygen content with respect to time (Figure 3f), the effect of temperature on the re-oxidation rate is obtained to further analyze the effect of the cooling rate on the re-oxidation degree. It could also observe two high-temperature re-oxidation peaks at about 997 °C and 800 °C-750 °C. The re-oxidation at higher temperatures is fast, implying that oxygen partial pressure is an important factor in the rate. The re-oxidation at low temperatures is slow, suggesting the temperature is also important. Despite the 50 °C hysteresis at 800 °C-750 °C in comparison to the temperature-elevating stage, the oxygen content and re-oxidation rate profiles on heating and cooling are almost entirely coincident with one another (Tables 3 and 4), indicating near equilibrium lattice oxygen release and uptake, and the phase stability of OC.

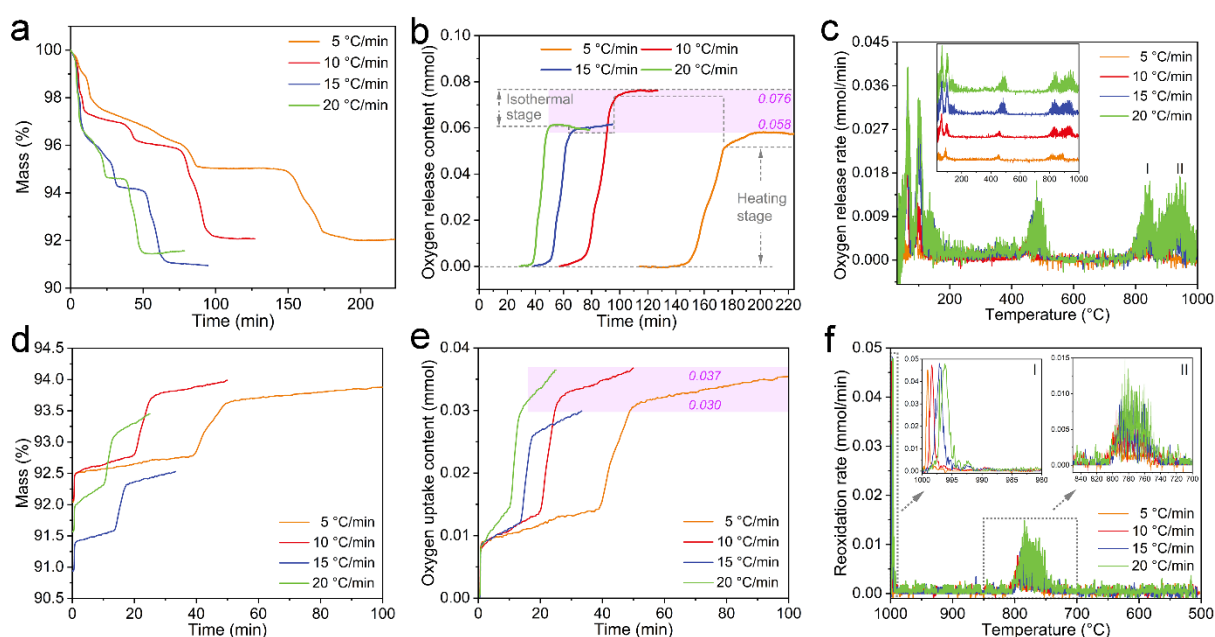


Figure 3. Redox performance of SCZ91 under different heating and cooling rates. (a) TG curves at the temperature-elevating stage, (b) variation of the lattice oxygen release content, (c) oxygen release rate of SCZ91 at different heating rates; (d) TG curves at re-oxidation stage, (e) variation of the oxygen uptake content, (f) oxygen uptake rate of SCZ91 at different cooling rates.

Table 3. Summary of weight loss, oxygen release content and oxygen release rate involving two peaks at the temperature-elevating stage from 600 to 1000 °C.

Rate (°C/min)	5	10	15	20
TG (%)	2.64	3.65	3.00	3.15
TG of peak I (%)	1.29	1.20	1.15	2.14
TG of peak II (%)	1.35	2.45	1.85	3.12
Oxygen release content (mmol)	0.057	0.076	0.062	0.059
Oxygen release content of peak I (mmol)	0.024	0.025	0.021	0.019
Oxygen release content of peak II (mmol)	0.033	0.051	0.041	0.040
Oxygen release rate of peak I (maximum, mmol/min)	0.003 (823 °C)	0.007 (836 °C)	0.008 (834 °C)	0.011 (938 °C)
Oxygen release rate of peak II (maximum, mmol/min)	0.004 (880 °C)	0.008 (936 °C)	0.009 (936 °C)	0.012 (946 °C)

Table 4. Summary of weight gain, oxygen uptake content and oxygen uptake rate involving two peaks at re-oxidation stage from 1000 to 500 °C.

Rate (°C/min)	5	10	15	20
TG (%)	1.84	1.91	1.58	1.89
TG of peak I (%)	0.75	0.71	0.65	0.75
TG of peak II (%)	1.09	1.20	0.93	1.14
Oxygen uptake content (mmol)	0.035	0.037	0.030	0.036
Oxygen uptake content of peak I (mmol)	0.014	0.014	0.012	0.014
Oxygen uptake content of peak II (mmol)	0.021	0.023	0.018	0.022
Oxygen uptake rate of peak I (maximum, mmol/min)	0.045 (999 °C)	0.048 (998 °C)	0.049 (997 °C)	0.048 (996 °C)
Oxygen uptake rate of peak II (maximum, mmol/min)	0.003 (795 °C)	0.006 (788 °C)	0.005 (784 °C)	0.008 (782 °C)

4. Conclusion

In summary, the oxygen release and redox stability of the cobalt-based perovskites, SrCoO_{3-δ} and SrCo_{0.9}Zr_{0.1}O_{3-δ} (SCZ91) as the potential STCS candidates, were investigated by XRD, FT-IR, Raman and TGA measurements. The XRD, FT-IR and Raman confirmed the dual-phase perovskite of SCZ91, i.e. SrCoO_{2.29} and SrZrO₃. The thermogravimetric analysis verified the incorporation of Zr could facilitate the oxygen release (0.071 mmol at step III) and enhance the phase stability compared to SCO, indicating the exceptional efficacy of SCZ91. The near-equilibrium lattice oxygen release and uptake at high temperatures could be observed through the redox performance of SCZ91 at different heating and cooling rates in N₂ and air. The results supported the further research for CO₂ splitting step using SCZ91 as oxygen exchange redox material.

Data availability statement

Data will be made available on request and fulfilled by the corresponding author.

Underlying and related material

None.

Author contributions

Liuqing Yang: Methodology, Investigation, Writing – review & editing, Formal analysis, Writing – original draft, Visualization. **Hui Liu:** Methodology, Formal analysis. **Jianan Hao:** Methodology, Validation, Investigation. **Junsheng Zhang:** Writing – review & editing, Validation, Supervision, Resources, Project administration, Methodology, Investigation, Funding acquisition, Conceptualization. **Jinjia Wei:** Writing – review & editing, Validation, Supervision, Resources, Project administration, Methodology, Investigation, Funding acquisition, Conceptualization.

Competing interests

The authors declare that they have no competing interests.

Funding

The authors gratefully acknowledge the support of this research work by the National Key R&D Program of China (2021YFF0500400), the National Natural Science Foundation of China (No.21978230), the Key Research Program of Shaanxi Province (2022GXLH-01-08), the Targeted Funding Program of Power Construction Corporation of China (DJ-PTZX-2021-03), and the Shaanxi Province Qin Chuangyuan "Scientist + Engineer" Team (2022KXJ-179).

References

1. M. I. Qadir, J. Dupont, "Thermo- and photocatalytic activation of CO₂ in ionic liquids nanodomains," *Angew. Chem.-Int. Edit.*, vol.62, no.31, pp. e202301497, Apr, 2023, doi: <https://doi.org/10.1002/anie.202301497>.
2. H. Jiang, L. Wang, H. Kaneko, R. Gu, G. Su, L. Li, J. Zhang, H. Song, F. Zhu, A. Yamaguchi, J. Xu, F. Liu, M. Miyauchi, W. Ding, M. Zhong, "Light-driven CO₂ methanation over Au-grafted Ce_{0.95}Ru_{0.05}O₂ solid-solution catalysts with activities approaching the thermodynamic limit", *Nat. Catal.*, vol.6, no.6, pp.519-530, Jun, 2023, doi: <https://doi.org/10.1038/s41929-023-00970-z>.
3. S. J. Davis, N. S. Lewis, M. Shaner, S. Aggarwal, D. Arent, I. L. Azevedo, S. M. Benson, T. Bradley, J. Brouwer, Y. M. Chiang, C. T. M. Clack, A. Cohen, S. Doig, J. Edmonds, P. Fennell, C. B. Field, B. Hannegan, B. M. Hodge, M. I. Hoffert, E. Ingersoll, P. Jaramillo, K. S. Lackner, K. J. Mach, M. Mastrandrea, J. Ogden, P. F. Peterson, D. L. Sanchez, D. Sperling, J. Stagner, J. E. Trancik, C. J. Yang, K. Caldeira, "Net-zero emissions energy systems", *Science*, vol.360, no.6396, pp.eaas9793, Jun, 2018, doi: <https://doi.org/doi:10.1126/science.aas9793>.
4. M. High, C. F. Patzschke, L. Zheng, D. Zeng, O. Gavalda-Diaz, N. Ding, K. H. H. Chien, Z. Zhang, G. E. Wilson, A. V. Berenov, S. J. Skinner, K. L. Sedransk Campbell, R. Xiao, P. S. Fennell, Q. Song, "Precursor engineering of hydrotalcite-derived redox sorbents for reversible and stable thermochemical oxygen storage", *Nat. Commun.*, vol.13, no.1, pp.5109, Aug, 2022, doi: <https://doi.org/10.1038/s41467-022-32593-6>.

- L. Zeng, Z. Cheng, J. A. Fan, L. S. Fan, J. Gong, "Metal oxide redox chemistry for chemical looping processes", *Nat. Rev. Chem.*, vol.2, no.11, pp.349-364, Nov, 2018, doi: <https://doi.org/10.1038/s41570-018-0046-2>.
- X. Qian, J. He, E. Mastronardo, B. Baldassarri, W. Yuan, C. Wolverton, S. M. Haile, "Outstanding properties and performance of $\text{CaTi}_{0.5}\text{Mn}_{0.5}\text{O}_{3-\delta}$ for solar-driven thermochemical hydrogen production", *Matter*, vol.4, no.2, pp.688-708, Feb, 2021, doi: <https://doi.org/10.1016/j.matt.2020.11.016>.
- Z. Chen, Q. Jiang, H. An, J. Zhang, S. Hao, X. Li, L. Cai, W. Yu, K. You, X. Zhu, C. Li, "Platinum group metal catalyst (RuO_x , PtO_x , and IrO_x)-decorated ceria-zirconia solid solution as high active oxygen carriers for solar thermochemical CO_2 splitting", *ACS Catal.*, vol.12, no.13, pp.7719-7736, Jun, 2022, doi: <https://doi.org/10.1021/acscatal.2c02044>.
- C. L. Muhich, B. W. Evanko, K. C. Weston, P. Lichty, X. Liang, J. Martinek, C. B. Musgrave, A. W. Weimer, "Efficient generation of H_2 by splitting water with an isothermal redox cycle", *Science*, vol.341, no.6145, pp.540-542, Aug, 2013, doi: <https://doi.org/doi:10.1126/science.1239454>.
- J. Hwang, R. R. Rao, L. Giordano, Y. Katayama, Y. Yu, Y. Shao-Horn, "Perovskites in catalysis and electrocatalysis", *Science*, vol.358, no.6364, pp.751-756, Nov, 2017, doi: <https://doi.org/10.1126/science.aam7092>.
- J. Vieten, B. Bulfin, P. Huck, M. Horton, D. Guban, L. Zhu, Y. Lu, K. A. Persson, M. Roeb, C. Sattler, "Materials design of perovskite solid solutions for thermochemical applications", *Energy Environ. Sci.*, vol.12, no.4, pp.1369-1384, Apr, 2019, doi: <https://doi.org/10.1039/C9EE00085B>.
- X. Qian, J. He, E. Mastronardo, B. Baldassarri, C. Wolverton, S. M. Haile, "Favorable redox thermodynamics of $\text{SrTi}_{0.5}\text{Mn}_{0.5}\text{O}_{3-\delta}$ in solar thermochemical water splitting", *Chem. Mat.*, vol.32, no.21, pp.9335-9346, Nov, 2020, doi: <https://doi.org/10.1021/acs.chemmater.0c03278>.
- L. Yang, Z. Zhao, C. Cui, J. Zhang, J. Wei, "Effect of nickel and cobalt doping on the redox performance of $\text{SrFeO}_{3-\delta}$ toward chemical looping dry reforming of methane", *Energy Fuels*, vol.37, no.16, pp.12045-12057, Jul, 2023, doi: <https://doi.org/10.1021/acs.energyfuels.3c01149>.
- Z. Zhang, L. Andre, S. Abanades, "Experimental assessment of oxygen exchange capacity and thermochemical redox cycle behavior of Ba and Sr series perovskites for solar energy storage", *Sol. Energy*, vol.134, pp.494-502, Sep, 2016, doi: <https://doi.org/10.1016/j.solener.2016.05.031>.
- R. Jacobs, J. Hwang, Y. Shao-Horn, D. Morgan, "Assessing correlations of perovskite catalytic performance with electronic structure descriptors", *Chem. Mat.*, vol.31, no.3, pp.785-797, Feb, 2019, doi: <https://doi.org/10.1021/acs.chemmater.8b03840>.
- L. Wang, T. Ma, S. Dai, T. Ren, Z. Chang, M. Fu, X. Li, Y. Li, "Solar thermochemical CO_2 splitting with doped perovskite $\text{LaCo}_{0.7}\text{Zr}_{0.3}\text{O}_3$: thermodynamic performance and solar-to-fuel efficiency", *RSC Adv.*, vol.10, no.59, pp.35740-35752, Sep, 2020, doi: <https://doi.org/10.1039/D0RA05709F>.
- L. Wang, T. Ma, S. Dai, T. Ren, Z. Chang, L. Dou, M. Fu, X. Li, "Experimental study on the high performance of Zr doped LaCoO_3 for solar thermochemical CO production", *Chem. Eng. J.*, vol.389, pp.124426, Jun, 2020, doi: <https://doi.org/10.1016/j.cej.2020.124426>.
- T. Akhtar, M. Anis-ur-Rehman, "Conductivity relaxations and phase purity in strontium cobalt oxides prepared by numerous chemical routes", *J. Dispersion Sci. Technol.*, vol.42, no.13, pp.1936-1949, Jul, 2020, doi: <https://doi.org/10.1080/01932691.2020.1791717>.
- L. Yang, J. Zhang, J. Wei, "Highly active $\text{La}_{0.35}\text{Sr}_{0.35}\text{Ba}_{0.3}\text{Fe}_{1-x}\text{Co}_x\text{O}_3$ oxygen carriers with the anchored nanoparticles for chemical looping dry reforming of methane", *Fuel*, vol. 349, pp.128771, Oct, 2023, doi: <https://doi.org/10.1016/j.fuel.2023.128771>.
- L. Yang, X. Li, X. Zhang, C. Huang, "Supercritical solvothermal synthesis and formation mechanism of V_2O_3 microspheres with excellent catalytic activity on the thermal

- decomposition of ammonium perchlorate", *J. Alloy. Compd.*, vol.806, pp.1394-1402, Oct, 2019, doi: <https://doi.org/10.1016/j.jallcom.2019.07.083>.
20. A. Glamazda, K. Y. Choi, P. Lemmens, W. S. Choi, H. Jeon, T. L. Meyer, H. N. Lee, "Structural instability of the CoO_4 tetrahedral chain in $\text{SrCoO}_{3-\delta}$ thin films", *J. Appl. Phys.*, vol. 118, no.8, pp. 085313, Aug, 2015, doi: <https://doi.org/10.1063/1.4929659>.
21. M. T. Azcondo, M. Orfila, M. Linares, R. Molina, J. Marugán, U. Amador, K. Boulahya, J. Á. Botas, R. Sanz, "Thermochemical energy storage using the phase transitions brownmillerite -2H perovskite - cubic perovskite in the $\text{Ca}_x\text{Sr}_{1-x}\text{CoO}_{3-\delta}$ ($x = 0$ and 0.5) system", *ACS Appl. Energ. Mater.*, vol.4, no.8, pp.7870-7881, Aug, 2021, doi: <https://doi.org/10.1021/acsaem.1c01235>.
22. M. Takacs, S. Ackermann, A. Bonk, M. Puttkamer, P. Haueter, J. R. Scheffe, U. F. Vogt, A. Steinfeld, "Splitting CO_2 with a ceria-based redox cycle in a solar-driven thermogravimetric analyzer", *AIChE J.*, vol.63, no.4, pp.1263-1271, Apr, 2017, doi: <https://doi.org/10.1002/aic.15501>.
23. F. Call, M. Roeb, M. Schmücker, C. Sattler, R. Pitz-Paal, "Ceria doped with zirconium and lanthanide oxides to enhance solar thermochemical production of fuels", *J. Phys. Chem. C*, vol.119, no.13, pp.6929-6938, Feb, 2015, doi: <https://doi.org/10.1021/jp508959y>.